Journal of Medicinal Chemistry Article

J. Med. Chem. **2009,** *52,* 6991–7002 **6991**
DOI: 10.1021/jm9003413

χ-Conopeptide Pharmacophore Development: Toward a Novel Class of Norepinephrine Transporter Inhibitor (Xen2174) for Pain[⊥]

Andreas Brust,*[,†,∥] Elka Palant,[†,∥] Daniel E. Croker,[†] Barbara Colless,[†] Roger Drinkwater,[†] Brad Patterson,[†] Christina I. Schroeder,[‡] David Wilson,[†] Carsten K. Nielsen,[§] Maree T. Smith,[§] Dianne Alewood,[†] Paul F. Alewood,[‡] and Richard J. Lewis*[,†,‡]

[†]*Xenome Ltd., 120 Meiers Road, Indooroopilly, Queensland, Australia 4068,* [‡]*Institute of Molecular Biosciences and* [§]*School of Pharmacy, The University of Queensland, Brisbane, Queensland, Australia.* [∥]*Equal first authors.*

Received March 17, 2009

Norepinephrine (NE) amplifies the strength of descending pain inhibition, giving inhibitors of spinal NET clinical utility in the management of pain. χ-MrIA isolated from the venom of a predatory marine snail noncompetitively inhibits NET and reverses allodynia in rat models of neuropathic pain. An analogue of χ-MrIA has been found to be a suitable drug candidate. On the basis of the NMR solution structure of this related peptide, Xen2174 (**3**), and structure−activity relationships of analogues, a pharmacophore model for the allosteric binding of **3** to NET is proposed. It is shown that **3** interacts with NET predominantly through amino acids in the first loop, forming a tight inverse turn presenting amino acids Tyr7, Lys8, and Leu9 in an orientation allowing for high affinity interaction with NET. The second loop interacts with a large hydrophobic pocket within the transporter. Analogues based on the pharmacophore demonstrated activities that support the proposed model. On the basis of improved chemical stability and a wide therapeutic index, **3** was selected for further development and is currently in phase II clinical trials.

Introduction

Marine natural products remain an important source of new chemical diversity for drug discovery.[1] The venom of the genus *Conus* (marine cone snails) provides an exceptionally rich source of highly evolved pharmacologically active compounds. These predatory mollusks are equipped with a venom apparatus that produces a species-specific cocktail of peptides to immobilize prey comprising fish, mollusks, and worms. It is estimated that the venom of a single *Conus* species may contain between 50 and 200 different venom components,[2] translating to more than 50 000 active peptides across the genus. Similar to spider and scorpion venoms, conopeptides are highly specific for their evolved target and frequently possess constrained structures containing multiple disulfide bonds. The disulfide framework is interspersed by loops of amino acids that define the binding motifs. The potency, selectivity, and chemical stability of venom peptides, particularly conopeptides, make these compounds attractive starting points for drug development.[3−6] In fact, several conotoxins are currently in clinical trials,[5] with one member of the ω-conotoxin family, MVIIA (ziconotide), on the market for the treatment of chronic pain.[7,8] On the basis of this potential, Xenome has developed a synthetic conopeptide library from nucleotide derived venom peptide sequences as a discovery platform for novel drug lead discovery.[9−12]

MrIA-OH (NGVCCGYKLCHOC-OH, aka mr10a and CMrVIB) and MrIB-OH (VGVCCGYKLCHOC-OH) are two closely related peptides that were discovered in the venom of the molluscivorous *Conus marmoreus*.[9,13,14] Sharpe et al. classified these peptides as χ-conopeptides based on activity displayed at the neuronal norepinephrine transporter (NET[a])

[⊥] This publication is dedicated to Dianne Alewood: gone too early and dearly missed by us all.

*To whom correspondence should be addressed. For A.B.: (phone) +617 3720 8055; (fax) +617 3720 8388; (e-mail) andreas.brust@xenome.com. For R.J.L.: (address) Xenome Ltd., 120 Meiers Road, Indooroopilly, Queensland, Australia; (phone) +61 7 3720 8055; (fax) +61 7 3720 8388; (e-mail) richard.lewis@xenome.com.

[a] Abbreviations: NET, norepinephrine transporter (aka noradrenaline transporter); NE, norepinephrine (aka noradrenaline); COO, ester bond; HBTU, *N*,*N*,*N*′,*N*′-tetramethyl-*O*-(1*H*-benzotriazol-1-yl)-uranium hexafluorophosphate; MSNT, 1-(2-mesitylensulfonyl)-3-nitro-1*H*-1,2,4-triazole; EDT, ethanedithiol; TIPS, triisopropylsilane; TFA, trifluoroacetic acid; DCC, *N*,*N*′-dicyclohexylcarbodiimide; NEM, *N*-ethylmorpholine; DMAP, 4-dimethylaminopyridine; DMSO, dimethyl sulfoxide; Acm, acetamidomethyl side chain protecting group for cysteine; RP-HPLC, reversed-phase high-performance liquid chromatography; LC−MS, liquid chromatography coupled mass spectrometry; NMR, nuclear magnetic resonance; NOESY, nuclear overhauser enhancement spectroscopy; TOCSY, total correlated spectroscopy; FIDs, free induction decays; DQF-COSY, double quantum filtered correlation spectroscopy; WATERGATE, water suppression by gradient-tailored excitation; E-COSY, exclusive correlation spectroscopy; GPCR, G-protein-coupled receptors; CCI, chronic constriction injury; IT, intrathecal; SAR, structure−activity relationship; SI, Supporting Information. Natural occurring amino acids are abbreviated to standard single or standard three letter codes: U represents L-pyroglutamic acid; O, L-*trans*-hydroxyproline. Capital letters represent L-amino acids, and lower case letters represent D-amino acids. Unnatural amino acids are indicated using a three letter code in brackets such as the following: [NAL], L-1-napthylalanine; [DMF], L-3,4-dimethoxyphenylalanine; [DPA], L-β,β-diphenylalanine; [HTY], L-homotyrosine; [HFE], L-homophenylalanine; [MEY], L-*O*-methyltyrosine; [CHA], L-cyclohexylalanine; [DMK], dimethyllysine; [ORN], ornithine; [HLY], L-homolysine; [NLE], L-norleucine; [CIT], L-citrulline; [NML], *N*-methyl-L-leucine; [FLA], L-2-furylalanine; [THI], L-2-thienylalanine; [PYA], L-3-pyridylalanine; [BTA], L-3-benzothienylalanine; [TIC], 1,2,3,4-L-tetrahydroisoquinoline-3-carboxylic acid; [HCY], L-homocysteine; [BHK], β-homolysine; [ABZ], 2-aminobenzoyl.

Published on Web 10/27/2009

in a noncompetitive (allosteric) manner.[9,15] NET reuptake inhibitors have potential in the treatment of neurological disorders such as depression,[16] schizophrenia,[17] anxiety,[18] chronic pain,[19,20] and other psychotic disorders.[21] The most prominent reuptake inhibitors are the tricyclic antidepressants (e.g., amitriptyline and imipramine), which inhibit both the serotonin and norepinephrine reuptake and are used systemically to treat major depressive disorders, generalized anxiety disorder, and neuropathic pain.[22]

The χ-conopeptides have two disulfide bonds connecting Cys1−Cys4 and Cys2−Cys3.[9] This arrangement of disulfide bonds is termed a "ribbon" fold and distinguishes the χ-conopeptides from other classes of conopeptides that possess a similar cysteine spacing but different cysteine connectivity as seen in the "globular" folded α- and ρ-conopeptides (Cys1−Cys3, Cys2−Cys4).[23] Amidated **1** (MrIA-NH_2) has slightly higher affinity at NET compared to the native peptide (MrIA-OH)[9] but maintains the same folding arrangement as determined by selective synthesis[13] and NMR spectroscopy.[24] The 3D NMR solution structure of **1** revealed that the rigid ribbon-framework formed by the disulfide bonds induces a β-hairpin with two antiparallel strands connected by an inverse γ-turn, the same motif originally observed in the NMR structure of **2** (MrIB).[9] On the basis of their higher affinity, all peptides investigated in this study were amidated at the C-terminus.

A systematic alanine scan of **1** revealed that Gly6, Tyr7, Lys8, and Leu9 which form the first intercysteine loop, and His11 in the second loop, are important for binding to NET.[15] With the use of NMR chemical shift analysis of **1** and comparison with the alanine scan mutants, a perturbation of the backbone structure was seen only upon replacement of Gly6. This suggested that the overall structure did not change except for the Gly6 analogue, indicating the side chain interactions of these amino acids with the transporter were important for high affinity interactions. In this study we conducted a detailed SAR analysis of χ-conopeptides and generated a pharmacophore model for their allosteric binding to NET. On the basis of superior chemical stability and its efficacy and side effect profile, **3** (Xen2174) was developed for clinical use.

Results and Discussion

Stability Assessment of 1. It is well-known that peptides containing an Asn residue at the N-terminus can undergo cyclization involving the β-carboxamide group. Figure 1A depicts the proposed mechanism of aspartimide formation with elimination of ammonia and subsequent hydrolytic ring-opening to yield the α- or β-aspartyl peptide, respectively, and a mass increase of 1 amu. The tendency toward deamidation is dependent on the primary and secondary structures of the peptide and the solvent.[25−27] It was reported that Asn−Gly and Asn−Ser sequences are far more prone to this reaction than sequences containing combinations of Asn with bulkier amino acids. **1** contains the reactive N-terminal Asn−Gly sequence with aspartimide conversion being observed during disulfide bond formation (pH 8.0 and pH 6.0) and upon storage in an acetate buffer (pH 5.4). Because of the difficult separation of **1** and the related α/β-aspartyl-peptides by HPLC, an exact time course of the conversion was difficult to determine. Mass spectrometry analysis of **1**, stored in acetate buffer (pH 5.4), monitored the aspartimide formation by measuring the decrease of peak height for the native peptide (MW = 1407.7) and the increase of the aspartimide analogue (MW = 1408.7) (Figure 1B).

With the observed N-terminal instability of **1**, analogues replacing the first residue were synthesized and tested to determine the importance of this residue on binding to NET.

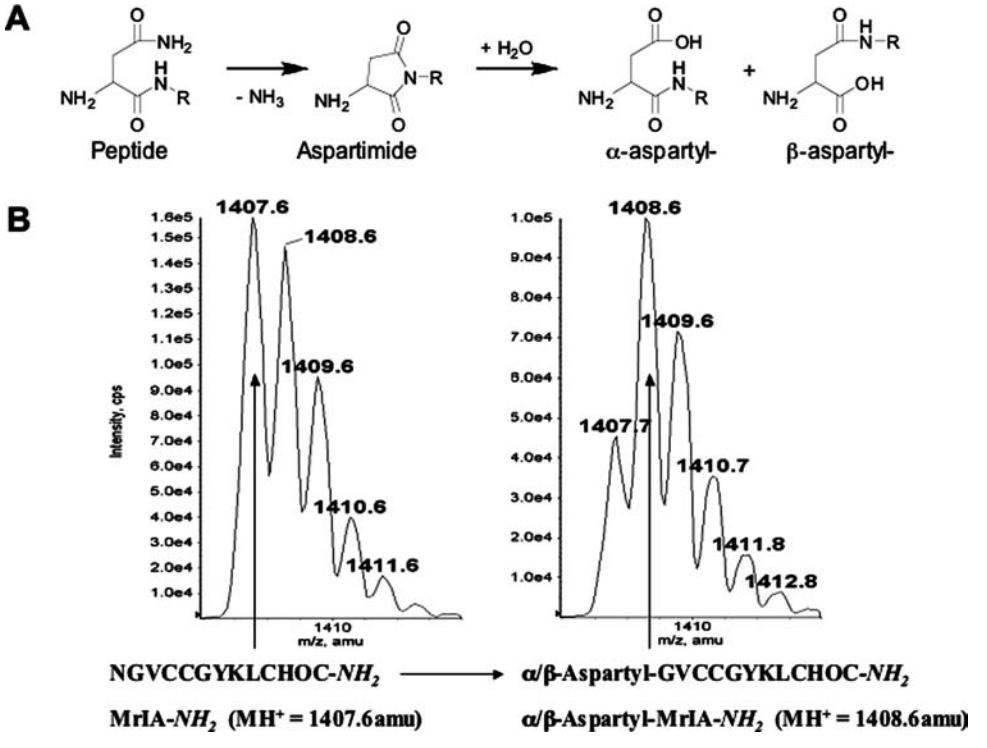

Figure 1. Aspartimide formation: (A) schematic representation of aspartimide formation in peptides containing N-terminal asparagine (Asn, N); (B) accurate mass measurement for **1** in acetate buffer (pH 5.4) at $t = 0$ days and $t = 6$ days. The conversion of native peptide (**1**) into the α/β-aspartyl analogues of **1** can be seen. [MH^+ 1407.6 amu (**1**); MH^+ 1408.6 amu (α/β-aspartyl-**1**)].

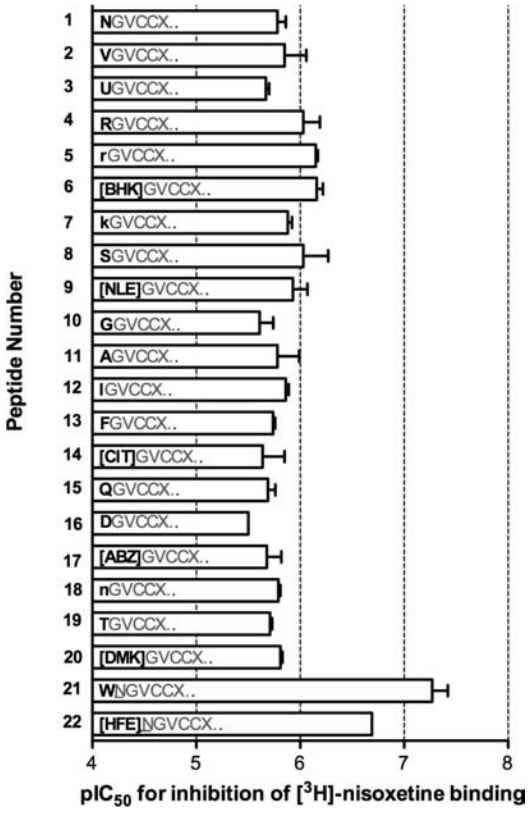

Figure 2. N-Terminal mutations of **1**. Shown are a series of analogues of **1** in which the N-terminal residues are replaced by various amino acids and assayed for inhibition of [^{3}H]nisoxetine binding to the human norepinephrine transporter (hNET) and corresponding affinity of the analogues compared to **1**. Amino acids in bold signify the point of difference from **1** and X... refers to the following sequence: GYKLCHOC. All peptides represented were synthesized as the C-terminal amide. Single letter abbreviations are used for standard L- or D-amino acids with unusual amino acids abbreviated with three letter codes and definitions available in the Abbreviations footnote. Bars represent the mean of two to five experiments performed in triplicate.

Improving the stability of this residue was seen to be critical for the further development of the peptide as a drug candidate. Extensive libraries of Asn1 mutants of **1** were produced by Fmoc solid phase chemistry. Random oxidation of purified reduced peptides was performed under the same conditions used for the synthesis of the native peptide with all peptides displaying a similar oxidation profile with the desired disulfide arrangement (Cys1−Cys4, Cys2−Cys3) corresponding to the second eluting isomer using HPLC conditions described. Figure 2 displays the binding affinities of the Asn-1 analogues of **1** for NET, presented as pIC_{50} values. All disulfide bond isomers generated during the synthesis process were submitted for assay. In all cases the second eluting main isomer displayed the highest binding affinity, and these isomers are compared and discussed.

The corresponding binding data of [Asn1]-**1** analogues, **4**−**20** (Figure 2), indicate that a number of amino acids are accommodated in the first position of the peptide with little compromise on affinity. With this in mind, further analogues were synthesized that extended the length of the chain by one amino acid to explore the pocket available for binding. From the in vitro binding data it can be seen that the addition of tryptophan and homophenylalanine, **21** and **22**, respectively, display enhanced affinity for NET.

Selection of 3 as a Preclinical Candidate. On the basis of obtained NET binding data (Figure 2), ease of synthesis, and peptide stability in buffer at pH7.4 (refer to SI), peptides **3**, **5**, **9**, **18**, **21**, and **22** were selected for assessment to establish efficacy, side effect profile, therapeutic window, and duration of action in an in vivo rat model of neuropathic pain (Figure 3). The unilateral chronic constriction injury (CCI) of the sciatic nerve rat model of neuropathic pain (CCI-rats)[28] was used to assess the ability of the analogues to attenuate mechanical allodynia, a hallmark symptom of neuropathic pain, in the ipsilateral (injured side) hindpaw. At 14 days after CCI surgery, each peptide of interest was administered as a bolus injection via a chronically implanted intrathecal (IT) cannula, with the positive and negative comparators in this study being morphine and vehicle respectively. In Figure 3 panels A−D summarize observed paw withdrawal threshold efficacy and time course for each tested compound, while panels E−M summarize compound related behavioral observations from assessments in CCI rats. From the animal data it is clear that 1 nmol of **1** produced similar efficacy as the lowest maximum efficacious dose of morphine (17.5 nmol) but fewer side effects. Compared with **1**, peptides **5**, **21**, and **22** produced greater side effects, **9** produced a similar extent of side effects, and **3** and **18** produced fewer side effects. Interestingly, **21** produced transient efficacy in the ipsilateral hindpaw, whereas the effects on the contralateral side were almost maximal and sustained, indicating a preferential effect on the undamaged side. Of the peptides producing similar or fewer side effects, efficacy was transient or of relatively short duration for **9** and **18**, respectively, whereas **3** produced a sustained response for 3 h that was equivalent to **1** at 3 h (albeit with a reduced maximal response). Dose−response studies confirmed that higher doses of **3** more than completely reversed allodynia and produced sustained efficacy beyond 24 h with little change in the side effect profile observed.[10] This superior side effect profile and efficacy, combined with the improved plasma stability of **3**, **5**, and **18** compared to **1** (refer to SI) has finally lead to selection of **3** as the most promising candidate for clinical development. A multiple target screen involving dopamine and serotonin transporters, opioid receptors, muscarinic receptors, and N-type calcium channel also indicated the high NET selectivity of **3** (refer to SI). Functional assays performed using human NET confirmed **3** as a norepinephrine uptake inhibitor ($\log IC_{50} = -6.7$; refer to SI).

NMR Structure of 3. A detailed SAR analysis was undertaken to help describe a pharmacophore model representing the interaction of **3** with NET. Previous alanine scan data on **1**[15] highlighted residues in loops 1 and 2 critical for binding to NET. To investigate these residues further, amino acids 6−9 in loop 1 and amino acids 11 and 12 in loop 2 of **3** were individually replaced with various amino acids sampling a wide range of side chain chemistry. Following the first generation of analogues, the more potent peptides from the series were further derivatized using closely related amino acids to fine-tune affinity and gain more detailed SAR information for the development of the pharmacophore model. A basic requirement to generate an interpretable pharmacophore model is a high resolution NMR structure. The NMR structure of **3** (Figure 4A) shows that the peptide adopts a tertiary structure very similar to the structures of **1**[24] and **2**,[9] as predicted from the Hα chemical shift comparison (Figure 4B). The structure of **3** comprised a ribbon-like fold

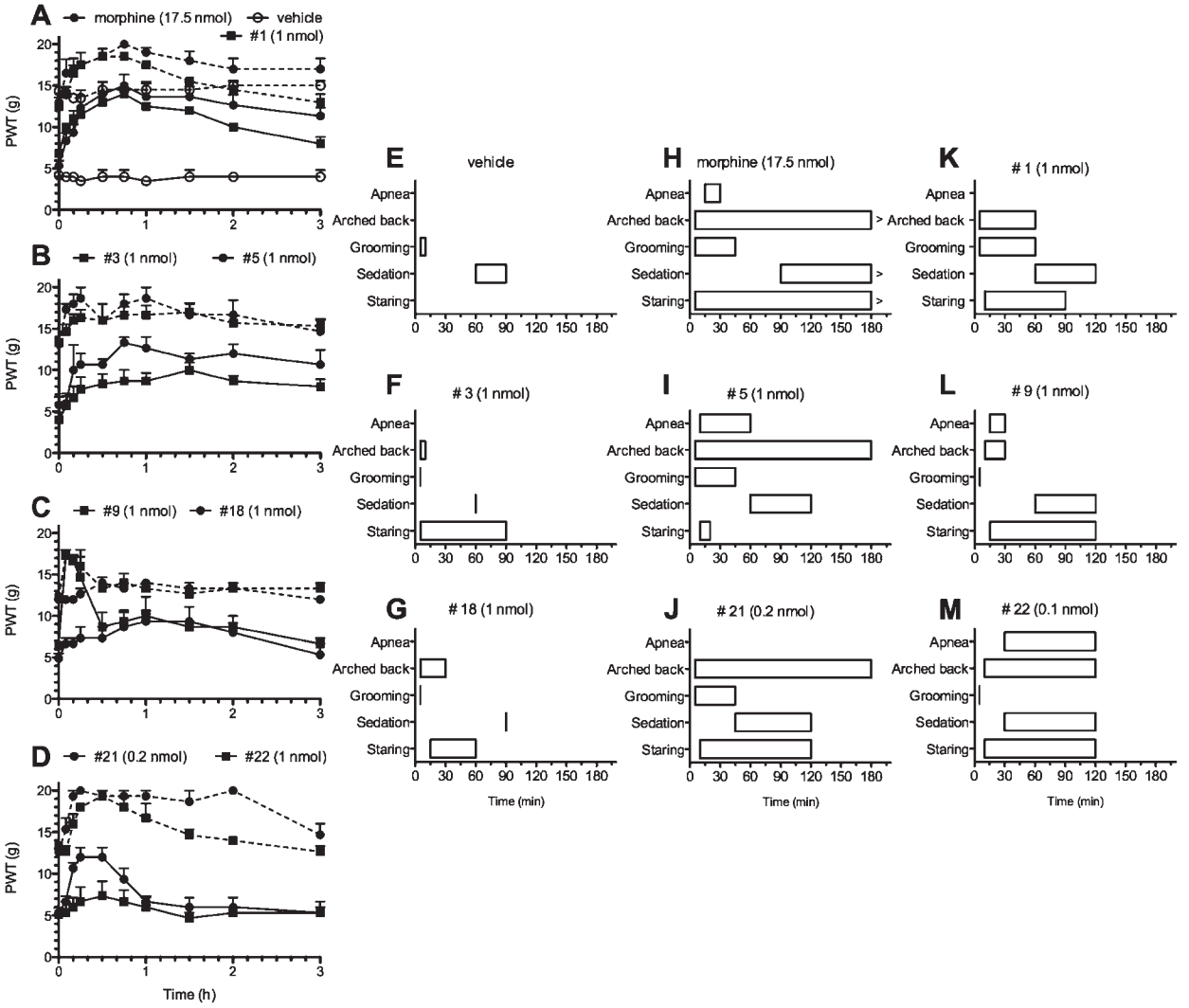

Figure 3. In vivo data (CCI rat pain model). Concentrations chosen for testing were based on binding affinity, with peptides **21** and **22** having higher binding affinity and thus tested at lower doses. The dose chosen for morphine is an efficacious dose. Peptides were administered as a single bolus injection via a cannula chronically implanted into the intrathecal space. Antinociception was assessed using calibrated von Frey filaments to determine changes in paw withdrawal thresholds in the hindpaw on the nerve damaged (ipsilateral) side relative to the corresponding measurements determined just prior to peptide administration. (A−D) Data for morphine,[10] vehicle,[10] and peptides **1**, **3**,[10] **5**, **9**, **18**, **21**, **22**; $N = 4-6$. Solid line represents data from the ipsilateral side and the dashed line from the contralateral (undamaged) side. The response to vehicle indicates the baseline sensitivity for the ipsilateral and contralateral hindpaws. (E−M) Observations from in vivo testing of selected peptides showing side effect profile using the CCI rat model of neuropathic pain. > indicates effects seen beyond 3 h time frame.

and a β-hairpin turn formed by residues 3−12, and an inverse γ-turn at residues 6−8 that connects the strands from residues 3−5 and 10−12. The observed hydrogen bonds in the structure of **3** were identified on the basis of distances and angles (Gly6-HN−Leu9-CO, Gly6-CO−Lys8-NH, Gly6-CO−Leu9-NH, His11-HN−Cys4-CO, and Cys4-HN−His11-CO). These identified hydrogen bonds corresponded to the slowly exchanging amide protons observed by NMR.

Secondary Hα chemical shifts of the various analogues of **3** were compared with that of **1** and **3** to determine if the differences seen in binding affinity were due to interactions within the binding site or to distortions in the backbone leading to changes in the overall fold of the peptide. To perform this study, secondary Hα chemical shifts were compared with random coil values[29] of individual amino acids within a peptide to gain a sensitive measure of backbone conformation.[30−32] For a series of structurally related peptides, secondary Hα chemical shift data can be used to identify the location but not the nature of local changes in backbone conformation.[33] Comparison of secondary Hα chemical shift data for **1** and **3** indicated that the backbone structures of both peptides are essentially identical (Figure 4B). In contrast to the disulfide-constrained portion of **1** and **3**, NMR analysis failed to define the N-terminal tail structure, indicating this region was likely poorly constrained in solution. Despite this region being less structured, most amino acid substitutions or additions to the N-terminus could increase binding affinity in particular for the N-terminal extended analogues **21** and **22** (Figure 2). Unfortunately, these changes increased the extent of side effects seen in the in vivo CCI rat model of neuropathic pain (Figure 3) believed to arise from off-target interactions. These peptides were not further investigated, as these changes in **21** and **22** represent an altered, extended pharmacophore accessing additional binding sites on NET and are potentially responsible also for off-site-related unwanted side effects, and hence, further analogues involving the N-terminal tail were not synthesized or further investigated.

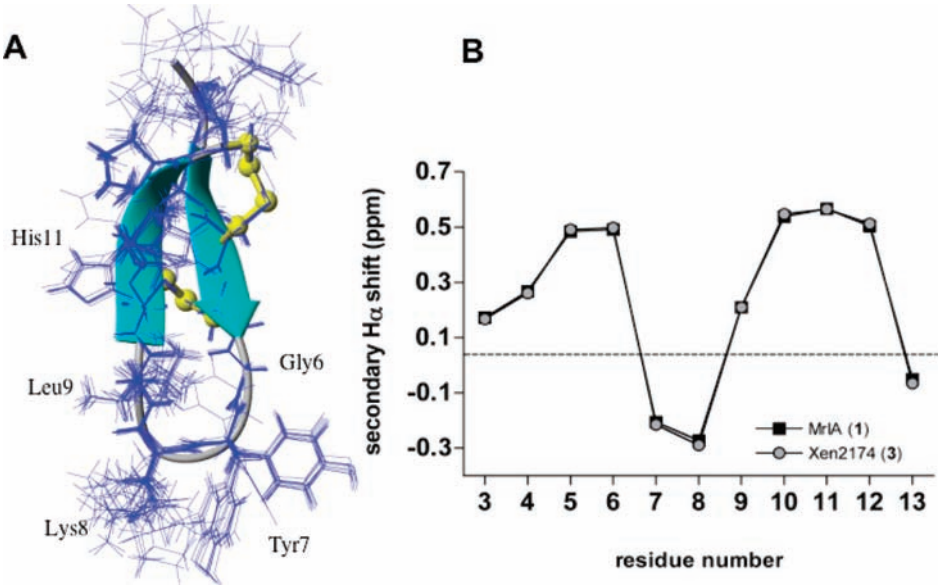

Figure 4. Structure of **3**: (A) superimposition of the 20 lowest energy structures for **3** calculated using high resolution NMR; (B) comparison of secondary Hα chemical shift data obtained for **1** and **3** indicating an identical backbone structure.

H-Bond Turn Stabilization. In previous work performed by Sharpe et al.[15] the [G6A]-**1** substitution was shown to have significantly reduced pharmacological activity at NET that appeared to correlate with a significant structural perturbation identified from the secondary Hα chemical shift data. The structural importance of this residue is further reflected, as it is conserved throughout the χ-conopeptide family. We believe that the Gly residue allows H-bond formation between Gly6-HN−Leu9-CO, Gly6-CO−Lys8-NH, and especially Gly6-CO−Leu9-NH. No Gly6 replacement with standard amino acids or D-Ala was able to maintain activity at NET (data not shown), and thus, no further mutations around this residue were pursued. To further probe the importance of loop stabilizing H-bonds in the peptide, in particular Gly6-CO to Leu9-NH, backbone modifications were introduced. To achieve this, the amide bond between Lys8 and Leu9 was replaced by an ester bond (**23**) or by N-methylation of the amide bond (**24**) (Figure 5). These modifications prevent the formation of the intramolecular Gly6-CO to Leu9-NH hydrogen bond due to a lack of a H-donor residue. The removal of the turn stabilizing H-bond resulted in total loss of activity of the depsi-peptide analogue (**23**) as measured by binding to NET. Furthermore, N-methylation of the Leu9-NH amide (**24**) removed the ability of this amide bond to act as a H-donor, resulting in loss of affinity at NET, along with pronounced backbone structure perturbation as seen in the secondary Hα chemical shift data for **24** (Figure 6). This led to the conclusion that the backbone H-bonds identified in **3** are essential for the overall stabilization of the hairpin scaffold in **3** and the ability to bind with high affinity to NET.

Tyr7 Residue Analogues. Analogues of **3** in which Tyr7 was replaced with a variety of amino acids were synthesized and assayed for NET binding (Figure 5, compounds **25**−**41**). These analogues included conservative substitutions such as phenylalanine (**28**), methyltyrosine (**29**), homotyrosine (**27**), and 2,4-dimethoxyphenylalanine (**25**), as well as nonconservative substitutions with acidic, basic, and hydrophobic amino acids. No inhibition was observed with these analogues with the exception of the *O*-methyltyrosine analogue, **29**, which maintained comparable potency to **3**. On comparison of the secondary Hα chemical shift data for selected Tyr7 mutants with **3** (Figure 6), some significant local perturbation for Lys8 was observed. For the analogue **36**, this was expected, as substitution with a proline has a significant structural effect on the backbone. However, the effects of Tyr7[HTY]-**3** (**27**) and Tyr7[CHA]-**3** (**30**) on the Hα proton of Lys8 were unexpected but may be explained by an interaction of the Tyr7 phenolic-OH and the Lys8-NH_2 as an additional backbone stabilizing factor. The inhibition of [^{3}H]nisoxetine from NET membrane for the Tyr7 analogues was reduced by even small changes such as the removal of the phenol function in tyrosine, Tyr7Phe-**3** (**28**), or the extension of the side chain by one CH_2 group, Tyr7[HTY]-**3** (**27**). There was also no binding for analogues with fused aromatic ring systems, Tyr7W-**3** (**31**) or Phe with a double methoxy substitution at the third and fourth position, Tyr7[DMF]-**3** (**25**), clearly highlighting a restricted binding pocket for Tyr7.

NMR analysis of the 20 lowest energy conformations of **3** revealed two thermodynamic preferred orientations of the aromatic tyrosine moiety. Although a low energy barrier separates the preferred orientations, considerations were given to investigate if both orientations are able to interact with NET. Diphenylalanine [DPA] was chosen to mimic simultaneous populations of both preferred orientations; however, this analogue, **26**, did not display a similar binding affinity to **3**. This indicated that the preferred orientation required for the tyrosine side chain at position 7 lies in a narrow spatial window.

Lys8 Residue Analogues. Analysis of position 8 in the NMR solution structure of **3** (Figure 4) revealed that the aliphatic linear aminobutyl side chain of Lys8 has a high degree of structural freedom. It is interesting to note that truncation or extension of the lysine side chain, **3** → **43** or **3** → **44**, respectively, abolished NET affinity. Even though the Lys side chain appears to have a high degree of structural freedom, the length of the freely rotating Lys chain is of greatest importance in regard to affinity displayed at NET. Further chemical diversity of this position was probed. However, none of the conservative substitutions (**42**−**45**)

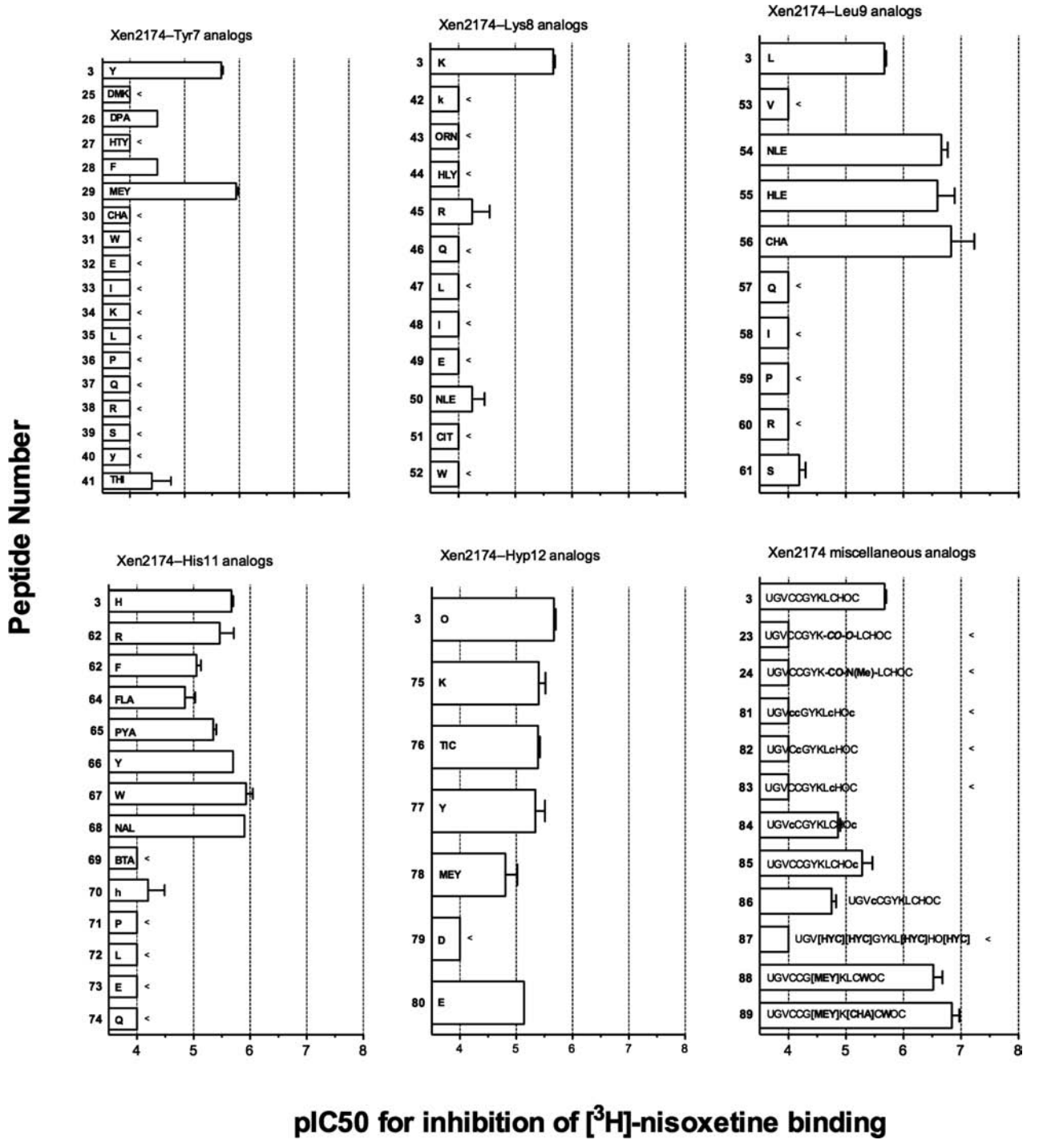

Figure 5. Analogues of **3** replacing various residues. The top bar represents **3** with the substituted residue in the bars below. Peptides were assayed for inhibition of [^{3}H]nisoxetine binding to human norepinephrine transporter and represented as pIC_{50} values. The potency of analogues with bars marked " < " represents estimates based on the lack of any inhibition detected at concentrations up to 100 μM. All peptides represented were synthesized as the C-terminal amide. Single letter abbreviations are used for standard L- or D-amino acids with unusual amino acids abbreviated with three letter codes, and definitions are available in the Abbreviations footnote. Bars represent the mean of two to five experiments performed in triplicate.

or the nonconservative substitutions (**46**−**52**) displayed activity at the NET. Secondary Hα chemical shift comparison of some Lys8 mutants showed an unchanged overall peptide backbone structure with the exception of a surprising perturbation of the backbone for the homolysine (**44**) analogue (Figure 6). This effect may be linked to the previously surmised H-bond interaction with the phenolic-OH function of Tyr7 acting to stabilize the structure.

Leu9 Residue Analogues. The aliphatic side chain of Leu9 displays a well-defined orientation projected orthogonally outward from the β-hairpin plane (Figure 4). It is apparent that the size of the aliphatic substitution plays a significant role in the affinity of **3** for NET, since the valine analogue **53** was unable to displace [^{3}H]nisoxetine while bulkier aliphatic residues including norleucine (**54**), homoleucine (**55**), or cyclohexylalanine (**56**) had increased affinity compared with

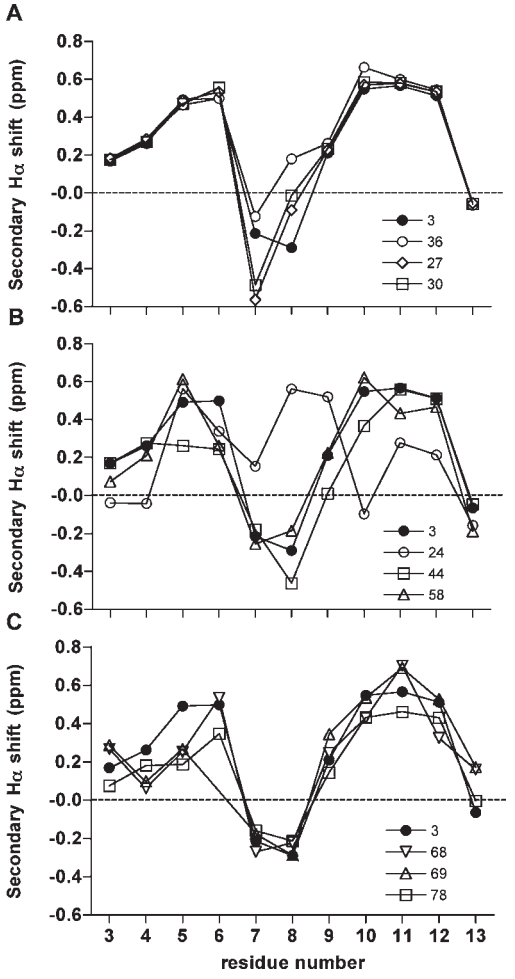

Figure 6. Secondary Hα chemical shifts (ppm) showing significant perturbations of various analogues compared to parent compound **3** represented in each of the panels by a closed circle. Panel A displays secondary Hα chemical shift (ppm) data for Tyr7 analogues, namely, Y7[HTY]-**3** (**27**), Tyr7[CHA]-**3** (**30**), and Y7P-**3** (**36**). Panel B displays secondary Hα chemical shift (ppm) data for Lys8 and Leu9 analogues, namely, K8[HLY]-**3** (**44**), L9[NML]-**3** (**24**), and L9I-**3** (**58**). Panel C displays secondary Hα chemical shift (ppm) data for His11 and Hyp12 analogues, namely, H11[NAL]-**3** (**68**), H11[BTA]-**3** (**69**), and O12[MEY]-**3** (**78**).

3, indicating that the aliphatic−hydrophobic binding patch is large enough to accommodate bulky aliphatic residues. No backbone conformational changes were observed in the secondary Hα chemical shift analysis for the Leu9 analogues (Figure 6), again highlighting the structural stability of the cysteine stabilized framework.

His11 Residue Analogues. The histidine imidazole moiety adopts an orientation parallel to Leu9, displaying essentially two main side chain conformations that project orthogonally out from the β-hairpin plane (Figure 4). This orientation is not maintained by the D-enantiomer analogue, **70**, resulting in decreased binding affinity compared to **3**. Screening of analogues **62**−**74** revealed that contribution of the histidine amino acid to affinity at NET is influenced by aromatic interactions as well by H-bond interactions from donor−acceptor sites. The five-ring aromatic substituted alanine, [FLA] (**64**), displayed similar binding affinity to **3**. Similar affinities to **3** were seen for six-ring aromatic analogues such as **63**, **65**, and **66** along with fused ring systems, such as **67** and **68** and the arginine analogue **62**. From the secondary Hα chemical shift data it can be seen that the larger fused ring analogues showed some distortions in the backbone. However, these were not in the important turn region between Gly6 and Leu9 but located toward the N-terminal tail region (Figure 3). The substitution of [BTA], L-3-benzothienylalanine (**69**), at position 11 did lead to perturbations in the turn backbone being reflected in loss of NET affinity (Figures 5 and 6).

Hyp12 Residue Analogues. Previous work[15] demonstrated that hydroxyproline (O) was not essential for χ-conopeptide binding to NET. This is surprising, as proline analogues usually have a strong structural effect, which often initiate turns because of the formation of a kink in the backbone forced by the cyclic structure. It was therefore unexpected that the overall fold of **3** is sufficiently stable that replacement of the turn-inducing cyclic Hyp (O) by an Ala residue is tolerated without significant loss of activity when compared to **3**. Furthermore, a variety of Hyp replacements (**75**−**80**), with the exception of aspartic acid (**79**), are tolerated without loss of binding affinity to NET. The SAR results in relation to the His position have shown that both basic and large aromatic residues are tolerated in this position. With this knowledge, replacements were made in **3** of the neighboring Hyp residue to the basic Lys (**75**) and aromatic amino acids like Tyr (**77**) or methyltyrosine (**78**). All these replacements maintained binding affinity at NET. Thus, similar to the neighboring His site, position 12 is able to accommodate a variety of residues including larger aromatic residues. This indicates that a large hydrophobic binding pocket can be accessed by loop 2 amino acids, framed by Cys3 and Cys4, in **3**. Secondary Hα shift analysis of **78** indicated that the mutation of hydroxyproline (**3**) to methyltyrosine (**78**) induced some minor backbone structural changes (Figure 6). However, these do not strongly influence the orientations of the key binding residues of loop 1, and thus, affinity is little altered.

Multiple Residue Replacement Analogues. The ribbon cysteine framework (1−4, 2−3) of the χ-conopeptides appears to be very stable, accommodating single amino acid mutations with little disruption to the backbone. The exception to this is the substitution of residues within the first loop with bulky residues, which creates minor distortions to the overall backbone observed in the secondary Hα chemical shift data presented above. It is anticipated that a change in the cysteine stereochemistry with the introduction of D-enantiomers would result in a disruption to the disulfide framework obtained after oxidation. Not surprisingly, replacement of the four L-Cys residues by D-Cys (**81**) caused complete loss of NET affinity. However, pairwise replacements with D-Cys produced unexpected effects. Cys1 and Cys4 replacement with D-Cys (**84**) was well tolerated, whereas the double D-Cys2 and D-Cys3 mutant (**82**) lost all affinity for NET. This finding suggests that Cys2 and Cys3 are critical to the stabilization of the inverse turn orientation of residues 6−9. It is hypothesized that a stereochemical variation in this scaffold bridge alters the topology of key binding residues, this being further supported by the single D-Cys mutants **83**, **85**, and **86**. When the four Cys residues were replaced with the methylene extended homocysteine [HCY], **87** was also not tolerated, perhaps because it increases torsional freedom of the disulfide scaffold, resulting in an altered backbone.

The information gained from the SAR analysis aided the design of analogues displaying greater affinity for NET

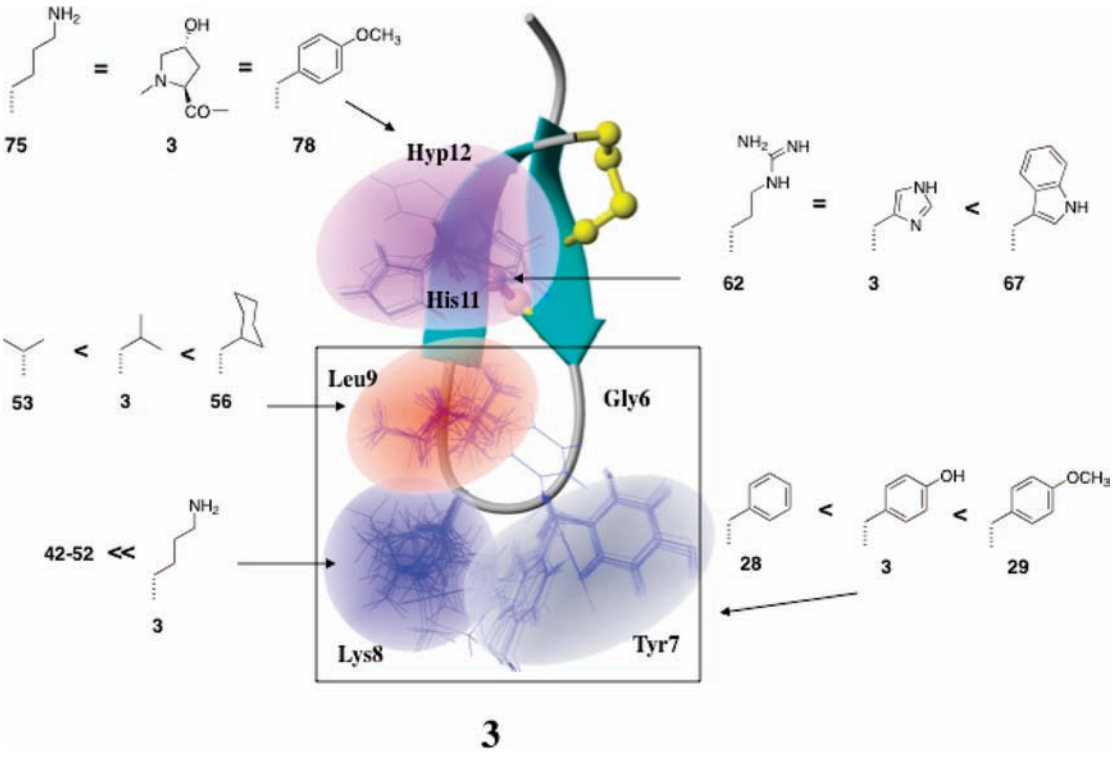

Figure 7. Proposed pharmacophore model of **3**. Important interaction sites are highlighted in color, with the framed turn region being crucial for activity at NET. The effect on potency of side chain modifications that drove the pharmacophore development compared with **3** is indicated, along with representative side chain substitutions. Gly6 has no direct pharmacophore contribution but immense importance for topology of the turn region (framed). The gray area represents the Tyr7 position interacting with NET via aromatic interactions as well as H-bond acceptor interaction. The blue area represents the Lys8 position with this being an essential basic residue for NET binding. The brown area represents the Leu9 position, which is able to assess a large hydrophobic patch on the norepinephrine transporter. The large purple area (His11−Hyp12) represents a site that can bind to the transporter via aromatic or basic interactions.

compared with **3**. Single amino acid substitutions such as Y7[MEY]-**3** (**29**) resulted in a slight increase in affinity, while larger aliphatic substitutions at position 9, for example, L9[CHA]-**3** (**56**), significantly enhanced affinity for the transporter in comparison with **3**. Other improvements in affinity were seen when His11 was substituted with larger aromatic residues such as tryptophan (**67**). To determine if these individual effects are additive, combinations of multiple amino acid analogues were designed. Both Y7[MEY]-**3** (**29**) and H11W-**3** (**67**) increased affinity by a small increment compared with **3**. Interestingly, when both of these substitutions were combined to form peptide Y7[MEY]-H11W-**3** (**88**), a 10-fold increase in affinity for the transporter was noted. The further substitution forming Y7[MEY]-L9[CHA]-H11W-**3** (**89**) increased binding affinity 20-fold compared with **3**. Binding affinity results for **88** clearly demonstrate that these multiple substitutions are more than additive. However, comparing peptide **89** with the single substitution of L9[CHA]-**3** (**56**) indicates that Y7[MEY] and H11W substitutions are not contributing significantly to the affinity for NET. It is not known if these changes in affinity are due to structural changes within the molecule and were not further investigated.

Pharmacophore Model of 3. By definition, χ-conopeptides contain two disulfide bonds with the connectivity being Cys1−Cys4 and Cys2−Cys3. In combination with the loop sizes of four amino acids in the first loop and two amino acids in the second loop, this disulfide bond arrangement and the multiple H-bonds result in a very stable core structure. As indicated from secondary Hα chemical shift experiments, the rigid hairpin-like conformation was generally maintained for those peptides, thus preserving activity at the transporter, despite the introduction of bulky residues at specific positions within the sequence. From these observations, it is believed that the action of **3** at the norepinephrine transporter does not require a conformational change to the backbone structure of the peptide to access the binding pocket. This allows for the development of a pharmacophore model based on the solution NMR structure in combination with NET affinity data (Figure 7).

Results from the SAR of **3** can be divided into three areas, each focusing on particular sections within the sequence. The first section relates to the N-terminal tail region of the peptide, which when modified did arrive at peptides (**21**, **22**) with higher binding affinity at the transporter compared with the parent molecule **3**. However, these modifications appeared to increase undesirable side effects without a concomitant increase in pain-relieving potency in the CCI rat model of neuropathic pain. It is hypothesized that the side effects are due to off-site effects. Increased binding to NET is caused when the additional introduced residues extending the pharmacophore and interacting with regions on the transporter are not accessible by the minimal pharmacophore of **3**. Replacement of the N-terminal Asn with pyroglutamic acid led to **3** with improved chemical stability as well as good efficacy and high potency when administered by the IT route in a widely utilized rat model of neuropathic pain at doses that were well-tolerated. On the basis of these improvements, **3** was progressed into preclinical and clinical development.

The second section relates to the second loop of the peptide corresponding to residues His11 and Hyp12. It was noted from the Ala scan data[15] that substitution of His11 with Ala reduced potency at the transporter whereas the substitution of Hyp12 with Ala did not significantly change potency compared to **1**. His11 and Hyp12 could be replaced by larger aromatic residues, suggesting that the binding pocket available to this section of **3** is somewhat larger. From the secondary Hα chemical shift data it would appear that the topology of these two residues is not critical to binding, as distortions in this region were tolerated. This can also be said for the two cysteines flanking the second loop, Cys4 and Cys13, where L-Cys to D-Cys changes were well tolerated.

The third section relates to the sensitive loop 1 turn region represented by the four amino acids, GYKL, which form the region of the peptide that is the most sensitive to topological alterations. From the Ala scan data it was seen that substituting any one of these amino acids with Ala abolished the activity at NET compared with the parent compound, **1**. The topology of these residues is restrained by the cysteine framework as well as an intraloop network of H-bonds. Tyr7 and Lys8 appear to be fundamental for binding to NET with limited allowable substitutions for Tyr7 ([MEY]) and no allowable substitutions found for Lys8, whereas Leu9 provided additional opportunities for improving affinity, with the introduction of larger aliphatic residues at this position enhancing potency.

Examination of the pharmacophore model (Figure 7) reveals that χ-conopeptides interact with the transporter from only one side of the hairpin-like turn, mainly residues Leu9 and His11 which protrude orthogonally outward. The other side of the peptide contains the disulfide bridges, which do not appear to be involved in binding to the transporter. Interestingly, all analogues with significantly higher affinity than **1** or **3** required the introduction of unnatural amino acids. Unfortunately, analogues at the N-terminus that had improved affinity for the transporter produced undesirable side effects and/or had reduced efficacy in the rat model of neuropathic pain. This study demonstrates that peptides found within venom can be optimized for therapeutic use. **1** identified in the venom of *Conus marmoreus* provided a suitable starting point for SAR studies and lead optimization. The resulting optimized clinical lead, **3**, has now entered phase II clinical trials.

Experimental Section

Materials. Protected Fmoc-amino acid derivatives were purchased from Novabiochem or Auspep P/L. The following side chain protected amino acids were used: Cys(Acm), Cys(Trt), His(Trt), Hyp(tBu), Tyr(tBu), Lys(Boc), Trp(Boc), Arg(Pbf), Asn(Trt), Asp(OtBu), Glu(OtBu), Gln(Trt), Ser(tBu), Thr(tBu), Tyr(tBu). All other Fmoc amino acids were unprotected. Unusual Fmoc amino acids [HTY], [ORN], [HLY], [CIT], and [BHK] were used with following side chain protections: −OH as −O^{t}Bu, −NH_2 as −NH(Boc), −COOH as −COO(^{t}Bu), and −SH as −S(Trt). All other unusual Fmoc amino acids were used unprotected. Unusual amino acids were sourced from Novabiochem, Auspep, CSPS-Pharmaceuticals, or NeoMPS. L-α-Hydroxyisovaleric acid was used unprotected. Dimethylformamide (DMF), dichloromethane (DCM), diisopropylethylamine (DIEA), and trifluoroacetic acid (TFA) were supplied by Auspep P/L (Melbourne, Australia) as peptide synthesis grade. 2-(1*H*-Benzotriazol-1-yl)-1,1,3,3-tetramethyluronium hexafluorophosphate (HBTU), triisopropylsilane (TIPS), HPLC grade acetonitrile, and methanol were supplied by Sigma Aldrich. The resin used was Fmoc-Rink resin (0.65 mmol/g) supplied by Auspep P/L, and Wang resin (0.81 mmol/g) was supplied by Novabiochem. Ethane dithiol (EDT) was supplied by Merck.

Synthetic Strategy. Peptide amides were synthesized on an Advanced ChemTech (ACT-396) automated peptide synthesizer using Rink amide resin (0.05 nmol). Peptide acids were synthesized on Wang resin loaded with the C-terminal Fmoc-Cys(Trt)-OH using MSNT/1-methylimidazole activation (4 equiv excess).[34] Continued assembly for the peptide acids as well as the complete assembly of peptide amides was performed using HBTU in situ activation protocols[35] to couple the Fmoc-protected amino acid to the resin (4 equiv excess). After chain assembly and final Fmoc deprotection the reaction block was transferred onto an ACT-LABTECH shaker and peptides were cleaved from the resin at room temperature (RT) in TFA/H_2O/TIPS/EDT (87.5:5:5:2.5) for 3 h. Cold diethyl ether (30 mL) was then added to the filtered cleavage mixture and the peptide precipitated. The precipitate was collected by centrifugation and subsequently washed with further cold diethyl ether to remove scavengers. The final product was dissolved in 50% aqueous acetonitrile and lyophilized to yield a fluffy white solid. The crude, reduced peptide was examined by reversed-phase HPLC for purity and the correct molecular weight confirmed by electrospray mass spectrometry (ESMS).

Synthesis of Ester Bond Containing Peptide 23. Peptide **23** was assembled using the above standard Fmoc protocol with the following exception. L-α-Hydroxyisovaleric acid was used instead of Fmoc-L-Leu-OH and coupled using DCC/NEM activation.[36] The ensuing formation of the ester bond between Fmoc-Lys(Boc)-OH and the hydroxy-peptide-resin was achieved after extended reaction times of 48 h using DCC/NEM/DMAP activation. Further continuation of assembly was performed using the described standard Fmoc protocol. Cleavage as well as oxidation was performed for peptide **23** under identical conditions to other peptides.

Random Disulfide Bond Formation in Peptides 1−89. Pure, reduced peptides (1 mg/mL) were oxidized by stirring at RT in 30% DMSO/0.1 M NH_4OAc, pH 6.0, for 16 h. The solutions were subsequently diluted to a DMSO concentration of < 5%, prior to RP-HPLC purification and lyophilization.

Selective Disulfide Bond Formation. Selectively folded MrIA-OH and MrIA-NH_2 were assembled on Wang (acid) and Rink (amide) resin, respectively. For each of the different isomers one pair of cysteine residues was incorporated into the sequence, using Cys(Trt) protection, while the other Cys pair used the orthogonal protection of Cys(Acm). After cleavage and purification of the reduced peptide the first disulfide bond was formed using the standard 30% DMSO/0.1 M NH_4OAc buffer (pH 6) method described above.

The formation of the second disulfide bond was performed by dissolving the purified, singly oxidized di-(Acm) peptide at 1 mM in 80% acetic acid/water. Iodine (10 equiv) dissolved in a small volume of ethyl acetate was added and the mixture stirred at RT. The progress of the Acm-deprotection and subsequent disulfide bond formation were monitored by direct injection ESMS at regular intervals until completion (approx 30−90 min). The reaction was then quenched by addition of ascorbic acid solution (10 mg/mL), resulting in a decolorization of the solution. After dilution with five times the volume of water and adjusting to pH 3, the fully oxidized peptide was loaded onto a RP-HPLC column and purified as described below.

HPLC Analysis and Purification. Analytical HPLC runs were performed using a Shimadzu HPLC system LC10A with a dual wavelength UV detector set at 214 and 254 nm. A reversed-phase C-18 column (Zorbax 300-SB C-18; 4.6 mm × 50 mm) with a flow rate of 2 mL/min was used. Gradient elution was performed with the following buffer systems: (solvent A) 0.05% TFA in water and (solvent B) 0.043% TFA in 90% acetonitrile

in water, from 0% B to 80% B in 20 min. The crude peptides and oxidized peptides were purified by semipreparative HPLC on a Shimadzu HPLC system LC8A associated with a reversed-phase C-18 column (Vydac C-18, 25 cm × 10 mm) running at a flow rate of 5 mL/min with a 1%/min gradient of 0% B to 40% B. The purity of the final product was evaluated by analytical HPLC (Zorbax 300SB C-18, 4.6 mm × 100 mm) with a flow rate of 1 mL/min and a 1.67%/min gradient of B (5−45%).

Purities of synthesized peptides (**1**, **3**, **5**−**8**, **10**, **12**, **17**, **20**, **22**−**24**, **30**, **35**, **43**, **45**, **49**, **53**, **54**, **56**, **59**, **60**−**62**, **65**−**67**, **71**, **72**, **74**−**76**, **81**, **83**−**88**) were all greater than 95% with the exceptions listed in the Support Information. The minor compounds in peptide samples consisted of other disulfide connectivity isomers that closely eluted to the desired 1−4, 2−3 connectivity isomer. Isolated minor isomers were also tested in the NET in vitro assay with none displaying affinity for the transporter.

Peptide Concentration Assessment. Peptide concentrations used in in vitro screening were calculated on the basis of peak size detected at 214 nm by HPLC. Peak size was calibrated using a peptide standard (in this case **1**) with known peptide content established by amino acid analysis. Molecular extinction coefficients are calculated for the standard, and the peptide of interest applying increments was established by Buck et al.[37] By use of the Lambert−Beer law, the peptide concentration is calculated on the basis of absorptions of standard and sample using calculated extinction coefficients.

Electrospray Mass Spectrometry (ESMS). Electrospray mass spectra were collected inline during analytical HPLC runs on an Applied Biosystems API-150 spectrometer operating in the positive ion mode with an OR of 20, Rng of 220, and Turbospray of 350°. Masses between 300 and 1800 amu were detected (step 0.2 amu, dwell 0.3 ms). Accurate mass measurement of the aspartimide formation of **1** (Figure 1B) was achieved by mass detection between 1402 amu and 1414 amu (step 0.1 amu, dwell 30 ms).

NMR Structure Evaluation of 3. Samples prepared for NMR spectroscopy contained approximately 7−8 mg of purified **3** dissolved in the following solvent systems: 95% H_2O/5% D_2O (v/v) at pH 3.38 and 99.96% D_2O. D_2O (99.96%) was obtained from Cambridge Isotope Laboratories, Woburn, MA. pH values were measured at 298 K, and no corrections for deuterium isotope effects were made.

Spectra were recorded on a Bruker ARX-500 or Bruker Advance 600 spectrometer at 290 and 298 K. The carrier frequency in all experiments was set at the center of the spectra on the water resonance frequency, and quadrature detection was used in both dimensions. 2D spectra were acquired in phase sensitive mode using time-proportional phase incrimination for quadrature detection in the t_1 dimension.[38] Exclusive homonuclear 2D experiments consisted of a DQF-COSY,[39] TOCSY[40] using a MLEV-17 spin lock sequence[41] with an isotropic mixing time of 80 ms, E-COSY,[42] and NOESY[43] with mixing times of 200 and 300 ms. Water suppression was achieved using a modified WATERGATE[44] sequence. All 2D spectra were collected with over 4096 data points in the F_2 dimension and 512 or 600 increments in the F_1 dimension. The presence of slowly exchanging amide protons were analyzed through a series of 1D and TOCSY spectra run immediately after dissolving the fully protonated sample in D_2O.

Spectra were processed on a Silicon Graphics workstation using XWINNMR (Bruker) software. The t_1 dimension was zero-filled to 2048 real data points, and 90° phase-shifted sine bell window functions were applied prior to Fourier transformation. Chemical shifts were referenced to internal sodium 2,2-dimethyl-2-silapentane-5-sulfonate (DSS). Processed spectra were analyzed and assigned within the program Sparky.[45] Assignment procedure followed the well-established spin system identification and sequential assignment technique.[46]

Structure Calculations. Cross-peaks from NOESY spectra recorded in 95% H_2O/5% D_2O with a mixing time of 300 ms were integrated and calibrated in Sparky[45] and distance constraints derived using CYANA.[47] Corrections for pseudoatoms were added to distance constraints where needed.[48] Backbone dihedral angle restraints were derived from $^3J_{HN\text{-}H\alpha}$ coupling constants measured from a one-dimensional spectrum or from line shape analysis of antiphase cross-peak splitting in the DQF-COSY spectrum. Angles were restrained following the standard parametrization of the Karplus relationship[46] to $-120 \pm 30°$ for $^3J_{HN\text{-}H\alpha}$ = 8.0−9.5 Hz (Val3, Cys4, Cys5, Leu9, Cys10, His11) and $-65 \pm 15°$ for $^3J_{HN\text{-}H\alpha}$ = 3.0−5.8 Hz (Cys13). An additional ϕ angle restraint of $-100 \pm 80°$ was applied to Tyr7 where the intraresidual $H_\alpha-H_N$ NOE was clearly weaker than the NOE between H_N and the H_α of the preceding residue.[49] The intense intraresidue $H_\alpha-H_N$ NOE for Lys8, combined with a $^3J_{HN\text{-}H\alpha}$ value of ~7 Hz, allowed its ϕ angle to be restrained to $+50 \pm 40°$.[50,51]

χ_1 dihedral angles were derived for three residues (Cys4, Cys10, Cys13) from $^3J_{\alpha\beta}$ coupling constants measured from E-COSY spectra in combination with $H_N-H_{\beta2}$, $H_N-H_{\beta3}$, $H_\alpha-H_{\beta2}$, and $H_\alpha-H_{\beta3}$ NOE peak intensities.[52] The χ_1 angles were restrained to $+180 \pm 30°$ (Cys4, Cys10) or $-60 \pm 30°$ (Cys13).

Preliminary structures were calculated using a torsion angle simulated annealing within CYANA.[47] Final structures were calculated using simulated annealing and energy minimization protocols within CNS, version 1.1.[53] The starting structures were generated using random (ϕ, ψ) dihedral angles and energy minimized to produce structures with the correct local geometry. A set of 50 structures were generated by a torsion angle simulated annealing protocol.[54,55] This protocol involves a high-temperature phase comprising 4000 steps of 0.015 ps of torsion angle dynamics, a cooling phase with 4000 steps of 0.015 ps of torsion angle dynamics during which the temperature is lowered to 0 K, and finally an energy minimization phase comprising 500 steps of Powell minimization. Structures consistent with restraints were subjected to further molecular dynamics and energy minimization in a water shell, as described by Linge and Nilges.[56] The refinement in explicit water involves the following steps: first, heating to 500 K via steps of 100 K, each comprising 50 steps of 0.005 ps of Cartesian dynamics; second, 2500 steps of 0.005 ps of Cartesian dynamics at 500 K before a cooling phase where the temperature is lowered in steps of 100 K, each comprising 2500 steps of 0.005 ps of Cartesian dynamics. Finally, the structures were minimized with 2000 steps of Powell minimization. Structures were analyzed using PROMOTIF[57] and PROCHECK-NMR.[58]

Chemical Shift Analysis of Analogues of 3. All spectra were recorded on a Bruker 600 Advance spectrometer equipped with an *x*, *y*, *z* gradient unit. Synthetic samples (~2−11 mM) were used for Hα chemical shift determinations. All samples were examined in 90% H_2O/10% D_2O (pH 3.5) except for **72** (His to [NAL] replacement) which required 20% CD_3CN to dissolve. Restraints acquired for Hα chemical shift determinations were from spectra recorded at 298 K. 1D proton NMR and 2D TOCSY[41] experiments were run for all peptides. For peptides that displayed differences in the backbone chemical shifts compared to **3**[15] and therefore could not be unambiguously assigned, additional NOESY[43] experiments were run. These peptides included **24**, **68**, **69**, and **82**. For all the other peptides, the residue replacements did not alter the backbone conformation and a TOCSY experiment provided satisfactory data for assignment of the Hα chemical shifts. All spectra were recorded using Bruker TopSpin in a phase sensitive mode over 12 ppm with 4096 data points in F2, 90−256 FIDs, 8−64 scans, and a recycle delay of 2.0 s. Water suppression for TOCSY and NOESY experiments was achieved using a modified WATERGATE sequence. Spectra were processed using XWINMR. The chemical shifts were referenced internally to DSS at 0.00 ppm and compared to the chemical shifts for amino acids in random coil, as described by Wüthrich.[46] Secondary shift changes of

> 0.1 ppm were considered as significant[59] and were used as an indication of structural perturbation upon amino acid mutations.

Radioligand Binding Studies. For radioligand binding studies, membranes from transfected COS-7 cells were incubated in 96-well plates with [^{3}H]nisoxetine (4.3 nM) in the absence or presence of χ-conopeptide (1 nM to 100 μM, in triplicate) in buffer for 1 h at RT, as previously described.[15] Filter-retained radioactivity was quantified by liquid scintillation counting. Curve fitting of concentration−response data was performed by nonlinear regression using individual data points with GraphPad Prism 3.0. The equation of Cheng and Prusoff[60] was used to convert IC_{50} values for [^{3}H]nisoxetine displacement to pK_i values, since χ-conopeptides act competitively with this ligand.[9] Statistical analyses were undertaken using the GraphPad Prism software package with a statistical significance criterion of $P < 0.05$.

In Vivo Studies. The CCI rat model of neuropathic pain was performed as described in Nielsen et al.[10] Three animals were used for each analogue tested, with dose selected on the basis of potency to inhibit the NET transport of NE.

Acknowledgment. We thank Norelle L. Daly for assistance in generation of the NMR structure and related graphics. This work was supported in part by an AusIndustry START Grant and an NHMRC Program Grant.

Supporting Information Available: HPLC purity data of all peptides, details of peptide quantification used in the determination of concentration used in in vitro assays, buffer and plasma stability data, receptor selectivity data of **3**, and in vitro functional assay results for **3**. This material is available free of charge via the Internet at http://pubs.acs.org.

References

(1) Newman, D. J.; Cragg, G. M. Marine natural products and related compounds in clinical and advanced preclinical trials. *J. Nat. Prod.* **2004**, *67*, 1216–1238.
(2) Jones, R. M.; Bulaj, G. Conotoxins. New vistas for peptide therapeutics. *Curr. Pharm. Des.* **2000**, *6*, 1249–1285.
(3) Armishaw, C. J.; Alewood, P. F. Conotoxins as research tools and drug leads. *Curr. Protein Pept. Sci.* **2005**, *6*, 221–240.
(4) Livett, B. G.; Gayler, K. R.; Khalil, Z. Drugs from the sea: conopeptides as potential therapeutics. *Curr. Med. Chem.* **2004**, *11*, 1715–1723.
(5) Alonso, D.; Khalil, Z.; Satkunanthan, N.; Livett, B. G. Drugs from the sea: conotoxins as drug leads for neuropathic pain and other neurological conditions. *Mini-Rev. Med. Chem.* **2003**, *3*, 785–787.
(6) Shen, G. S.; Layer, R. T.; McCabe, R. T. Conopeptides: from deadly venoms to novel therapeutics. *Drug Discovery Today* **2000**, *3*, 98–106.
(7) Garber, K. Peptide leads new class of chronic pain drugs. *Nat. Biotechnol.* **2005**, *23*, 399.
(8) Wermeling, D. P.; Berger, J. R. Ziconotide infusion for severe chronic pain: case series of patients with neuropathic pain. *Pharmacotherapy* **2006**, *26*, 395–402.
(9) Sharpe, I. A.; Gehrmann, J.; Loughnan, M. L.; Thomas, L.; Adams, D. A.; Atkins, A.; Palant, E.; Craik, D. J.; Adams, D. J.; Alewood, P. F.; Lewis, R. J. Two new classes of conopeptides inhibit the alpha 1-adrenoceptor and noradrenaline transporter. *Nat. Neurosci.* **2001**, *4*, 902–907.
(10) Nielsen, C. K.; Lewis, R. J.; Alewood, D.; Drinkwater, R.; Palant, E.; Patterson, M.; Yaksh, T. L.; McCumber, D.; Smith, M. T. Antiallodynic efficacy of the chi-conopeptide, Xen2174, in rats with neuropathic pain. *Pain* **2005**, *118*, 112–124.
(11) Lima, V.; Mueller, A.; Kamikihara, S. Y.; Raymundi, V.; Alewood, D.; Lewis, R. J.; Chen, X.; Minneman, K. P.; Pupo, A. S. Differential antagonism by conotoxin rho-TIA of contractions mediated by distinct alpha1-adrenoceptor subtypes in rat vas deferens, spleen and aorta. *Eur. J. Pharmacol.* **2005**, *508*, 183–192.
(12) Lewis, R. J.; Garcia, M. L. Therapeutic potential of venom peptides. *Nat. Rev. Drug Discovery* **2003**, *2*, 790–802.
(13) McIntosh, J. M.; Corpuz, G. O.; Layer, R. T.; Garrett, J. E.; Wagstaff, J. D.; Bulaj, G.; Vyazovkina, A.; Yoshikami, D.; Cruz, L. J.; Olivera, B. M. Isolation and characterization of a novel conus peptide with apparent antinociceptive activity. *J. Biol. Chem.* **2000**, *275* (42), 32391–32397.
(14) Balaji, R. A.; Ohtake, A.; Sato, K.; Gopalakrishnakone, P.; Kini, R. M.; Seow, K. T.; Bay, B.-H. α-Conotoxins, a new family of conotoxins with unique disulfide pattern and protein folding. *J. Biol. Chem.* **2000**, *275* (50), 39516–39522.
(15) Sharpe, I. A.; Palant, E.; Schroeder, C. I.; Kaye, D. M.; Adams, D. J.; Alewood, P. F.; Lewis, R. J. Inhibition of the norepinephrine transporter by the venom peptide chi-MrIA. Site of action, Na^+ dependence, and structure−activity relationship. *J. Biol. Chem.* **2003**, *278*, 40317–40323.
(16) Brunello, N. J.; Mendlewicz, J.; Kasper, S.; Leonard, B.; Montgomery, S.; Nelson, J.; Paykel, E.; Versiani, M.; Racagni, G. The role of noradrenaline and selective noradrenaline reuptake inhibition in depression. *Eur. Neuropsychopharmacol.* **2002**, *12*, 461–475.
(17) Arnsten, A. F. Adrenergic targets for the treatment of cognitive deficits in schizophrenia. *Psychopharmcology (Berlin)* **2004**, *174*, 25–31.
(18) Tanaka, M.; Yoshida, M.; Emoto, H.; Ishii, H. Noradrenaline systems in the hypothalamus, amygdala and locus coeruleus are involved in the provocation of anxiety: basic studies. *Eur. J. Pharmacol.* **2000**, *405*, 397–406.
(19) Drummond, P. D. Noradrenaline increases hyperalgesia to heat in skin sensitised by capsaicin. *Pain* **1995**, *60*, 311–315.
(20) Furst, S. Transmitters in antinociception in the spinal cord. *Brain Res. Bull.* **1999**, *48*, 129–141.
(21) Ressler, K. J.; Nemeroff, C. B. Role of norepinephrine in the pathophysiology and treatment of mood disorders. *Biol. Psychiatry* **1999**, *46*, 1219–1223.
(22) Ziegler, D. Painful diabetic neuropathy: treatment and future aspects. *Diabetes/Metab. Res. Rev.* **2008**, *24* (S1), S52–S57.
(23) Kang, T. S.; Radic, Z.; Talley, T. T.; Jois, S. D. S.; Taylor, P.; Kini, R. M. Protein folding determinants: structural features determining alternative disulfide pairing in α- and χ/λ-conotoxins. *Biochemistry* **2007**, *46*, 3338–3355.
(24) Nilsson, K. P. R.; Lovelace, E. S.; Caesar, C. E.; Tynngard, N.; Alewood, P. F.; Johansson, H. M.; Sharpe, I. A.; Lewis, R. J.; Daly, N. L.; Craik, D. J. Solution structure of χ-conopeptide MrIA, a modulator of the human norepinephrine transporter. *Pept. Sci.* **2005**, *80*, 815–823 (PDB 2ew4) .
(25) Blankemeyer-Menge, B.; Nimtz, M.; Frank, R. An efficient method for anchoring Fmoc-amino acids to hydoxyl-functionalised solid supports. *Tetrahedron Lett.* **1990**, *31*, 1701–1704.
(26) Schnolzer, M.; Alewood, P.; Jones, A.; Alewood, D.; Kent, S. B. In situ neutralization in Boc-chemistry solid phase peptide synthesis. Rapid, high yield assembly of difficult sequences. *Int. J. Pept. Protein Res.* **1992**, *40*, 180–193.
(27) Blankenship, J. W.; Balambika, R.; Dawson, P. E. Probing backbone hydrogen bonds in the hydrophobic core of GCN4. *Biochemistry* **2002**, *41*, 15676–15684.
(28) Bennett, G. J.; Xie, Y. K. A peripheral mononeuropathy in rat that produces disorders of pain sensation like those seen in man. *Pain* **1988**, *33*, 87–107.
(29) Stein, E. G.; Rice, L. M.; Brunger, A. T. Torsion-angle molecular dynamics as a new efficient tool for NMR structure calculation. *J. Magn. Reson.* **1997**, *124*, 154–164.
(30) Brooks, B. R.; Bruccoleri, R. E.; Olafson, B. D.; States, D. J.; Swaminathan, S.; Karplus, M. CHARMM: a program for macromolecular energy, minimization, and dynamics calculations. *J. Comput. Chem.* **2004**, *4*, 187–217.
(31) Hyberts, S. G.; Goldberg, M. S.; Havel, T. F.; Wagner, G. The solution structure of eglin c based on measurements of many NOEs and coupling constants and its comparison with X-ray structures. *Protein Sci.* **1992**, *1*, 736–751.
(32) Gehrmann, J.; Alewood, P. F.; Craik, D. J. Structure determination of the three disulphide bond isomers of α-conotoxin GI: a model for the role of disulphide bonds in structural stability. *J. Mol. Biol.* **1998**, *278*, 401–415.
(33) Nielsen, K. J.; Skjaerbaek, N.; Dooley, M.; Adams, D. A.; Martensen, M.; Dodd, P. R.; Craik, D. J.; Alewood, P. F.; Lewis, R. J. Structure−activity studies of conantokins as human *N*-methyl-D-aspartate receptor modulators. *J. Med. Chem.* **1999**, *42*, 415–426.
(34) Blankemeyer-Menge, B.; Nimtz, M.; Frank, R. An efficient method for anchoring Fmoc-amino acids to hydroxyl-functionalised solid supports. *Tetrahedron Lett.* **1990**, *31*, 1701–1704.
(35) Schnölzer, M.; Alewood, P.; Jones, A.; Alewood, D.; Kent, S. B. In situ neutralization in Boc-chemistry solid phase peptide synthesis. Rapid, high yield assembly of difficult sequences. *Int. J. Pept. Protein Res.* **1992**, *40* (3−4), 180–193.
(36) Blankenship, J. W.; Balambika, R.; Dawson, P. E. Probing backbone hydrogen bonds in the hydrophobic core of GCN4. *Biochemistry* **2002**, *41* (52), 15676–15684.

(37) Buck, M. A.; Olah, T. A.; Weitzmann, C. A.; Cooperman, B. S. Protein estimation by the product of integrated peak area and flow rate. *Anal. Biochem.* **1989**, *182*, 295–299.
(38) Marion, D.; Wüthrich, K. Application of phase sensitive two-dimensional correlated spectroscopy (COSY) for measurements of $^{1}H-^{1}H$ spin−spin coupling constants in proteins. *Biochem. Biophys. Res. Commun.* **1983**, *113* (3), 967–974.
(39) Rance, M.; Sorensen, O. W.; Bodenhausen, G.; Wagner, G.; Ernst, R. R.; Wüthrich, K. Improved spectral resolution in COSY ^{1}H NMR spectra of proteins via double quantum filtering. *Biochem. Biophys. Res. Commun.* **1983**, *117* (2), 479–485.
(40) Braunschweiler, L.; Ernst, R. R. Coherence transfer by isotropic mixing: application to proton correlation spectroscopy. *J. Magn. Reson.* **1983**, *53* (3), 521–528.
(41) Bax, A.; Davis, D. G. MLEV-17-based two-dimensional homonuclear magnetization transfer spectroscopy. *J. Magn. Reson.* **1985**, *65* (2), 355–360.
(42) Griesinger, C.; Sorensen, O. W.; Ernst, R. R. Practical aspects of the ECOSY technique. Measurement of scalar spin−spin coupling constants of peptides. *J. Magn. Reson.* **1987**, *75* (3), 474–492.
(43) Jeener, J.; Meier, B. H.; Bachmann, P.; Ernst, R. R. Investigation of exchange processes by two-dimensional NMR spectroscopy. *J. Chem. Phys.* **1979**, *71* (11), 4546–4553.
(44) Piotto, M.; Saudek, V.; Sklenar, V. Gradient-tailored excitation for single runtime NMR spectroscopy of aqueous solutions. *J. Biomol. NMR* **1992**, *2* (6), 661–665.
(45) Goddard, T. D.; Kneller, D. G. *SPARKY 3 NMR Software*; University of California: San Francisco, CA.
(46) Wüthrich, K. *NMR of Proteins and Nucleic Acids*; Wiley-Interscience: New York, 1986.
(47) Güntert, P.; Mumenthaler, C.; Wüthrich, K. Torsion angle dynamics for NMR structure calculation with the new program DYANA. *J. Mol. Biol.* **1997**, *273* (1), 283–298.
(48) Wüthrich, K.; Billeter, M.; Braun, W. Pseudo-structures for the 20 common amino acids for use in studies of protein conformations by measurements of intramolecular proton−proton distance constraints with nuclear magnetic resonance. *J. Mol. Biol.* **1983**, *169* (4), 949–961.
(49) Clubb, R. T.; Ferguson, S. B.; Walsh, C. T.; Wagner, G. Three-dimensional solution structure of *Escherichia coli* periplasmic cyclophilin. *Biochemistry* **1994**, *33* (10), 2761–2772.
(50) Omecinsky, D. O.; Holub, K. E.; Adams, M. E.; Reily, M. D. Three-dimensional structure analysis of mu-agatoxins: further evidence for common motifs among neurotoxins with diverse ion channel specificities. *Biochemistry* **1996**, *35* (9), 2836–2844.
(51) Ludvigsen, S.; Poulsen, F. M. Positive theta-angles in proteins by nuclear magnetic resonance spectroscopy. *J. Biomol. NMR* **1992**, *2* (3), 227–233.
(52) Wagner, G.; Braun, W.; Havel, T. F.; Schaumann, T.; Go, N.; Wüthrich, K. Protein structures in solution by nuclear magnetic resonance and distance geometry. The polypeptide fold of the basic pancreatic trypsin inhibitor determined using two different algorithms, DISGEO and DISMAN. *J. Mol. Biol.* **1987**, *196* (3), 611–639.
(53) Brünger, A. T.; Adams, P. D.; Rice, L. M. New applications of simulated annealing in X-ray crystallography and solution NMR. *Structure* **1997**, *5* (3), 325–336.
(54) Rice, L. M.; Brünger, A. T. Torsion angle dynamics: reduced variable conformational sampling enhances crystallographic structure refinement. *Proteins* **1994**, *19* (4), 277–290.
(55) Stein, E. G.; Rice, L. M.; Brünger, A. T. Torsion-angle molecular dynamics as a new efficient tool for NMR structure calculation. *J. Magn. Reson.* **1997**, *124* (1), 154–164.
(56) Linge, J. P.; Nilges, M. Influence of non-bonded parameters on the quality of NMR structures: a new force field for NMR structure calculation. *J. Biomol. NMR* **1999**, *13* (1), 51–59.
(57) Hutchinson, E. G.; Thornton, J. M. PROMOTIF, a program to identify and analyze structural motifs in proteins. *Protein Sci.* **1996**, *5* (2), 212–220.
(58) Laskowski, R. A.; Rullmannn, J. A.; MacArthur, M. W.; Kaptein, R.; Thornton, J. M. AQUA and PROCHECK-NMR: programs for checking the quality of protein structures solved by NMR. *J. Biomol. NMR* **1996**, *8* (4), 477–486.
(59) Wishard, D. S.; Sykes, B. D.; Richards, F. M. The chemical shift index: a fast and simple method for the assignment of protein secondary structure through NMR spectroscopy. *Biochemistry* **1992**, *31*, 1647–1651.
(60) Cheng, Y.; Prusoff, W. H. Relationship between the inhibition constant (K_i) and the concentration of inhibitor which causes 50% inhibition (I_{50}) of an enzymatic reaction. *Biochem. Pharmacol.* **1973**, *22* (23), 3099–3108.